2009 IEEE International Conference on Robotics and Automation
Kobe International Conference Center
Kobe, Japan, May 12-17, 2009

Dynamic Modeling and Analysis of Pitch Motion of a Basilisk Lizard Inspired Quadruped Robot Running on Water

Hyun Soo Park, Steven Floyd, and Metin Sitti
NanoRobotics Laboratory, Department of Mechanical Engineering,
Carnegie Mellon University, Pittsburgh, PA 15213

***Abstract*— A quadrupedal robot inspired by the basilisk lizard was developed and modeled with a 3-D real time simulation. Due to the robot's geometry, leg motion, and water interactions, the net pitch moment at the center of mass is not zero making pitch motion unstable. This paper introduces two types of tails, passive and active, to stabilize pitch motion and analyzes the advantages and disadvantages of each. It is shown in simulation that a purely passive tail can stabilize pitch motion and lead to a steady state robot pitch angle in the absence of disturbances. It is further shown that an active tail can compensate for disturbances and correct any drift in the robot body pitch angle due to changes in robot running speed.**

I. Introduction

Small animals and insects utilize diverse methods to float and locomote upon a water's surface. For example, water striders and spiders, which are very light-weight insects, use surface tension [1], [2]. Heavier animals, such as basilisk lizards, predominantly use the drag forces exerted by the fast motion of their feet on the water, and take advantage of hydrodynamics for locomotion [3], [4]. A basilisk lizard's ability to locomote on both land and water using the same legged running mechanism would be a desirable trait for mimicry in robots. A robot with such an ability would provide insight into both nature and potential robotics applications.

Bio-inspired robots are machines which emulate some aspect of a living system. This work describes the dynamics of a biomimetic robot which runs on the surface of water in a manner similar to a basilisk lizard. Unlike other aquatic and amphibious robots which must swim or walk through the water [5]–[8], the water runner can stride upon it. This robot employs momentum transfer for both lift and propulsion, with negligible use of surface tension or buoyancy, which other water walking robots employ [9]–[11]. Hence, this robot is the lightest of the amphibious robots, but the heaviest of the robots which locomote by water walking.

In previous studies, a basilisk lizard inspired quadruped robot that is capable of locomotion on the water's surface was devised and examined [4], [12]–[14]. This robot can run across the surface of water by slapping and stroking its feet quickly through the water, creating a short lived air cavity, and using the generated hydrodynamic and hydrostatic lift forces to propel itself. Based on experimental work, a 3-D simulation was developed to analyze both the lifting force and roll motion of the robot. Analysis of the lifting force showed the robot was capable of running on water using viscous drag forces and provided a criterion for convergence to a steady state distance from the water. The roll motion analysis examined stability in the roll direction, and determined the required roll moment of inertia to stably locomote on water as a function of the running frequency using a pendulum modeling analysis.

A key problem of the water runner is an instability of the pitch motion which causes the robot to flip backward. This is due to a net pitch moment generated by the lift and thrust forces of each of the four feet. Unlike other quadrupedal robots, the water runner has few degrees of freedom, which makes actively changing the center of mass a difficult proposition. Instead, a tail is added to the robot to generate a pitch moment in the opposite direction. The operation and effectiveness of both a passive and active tail are modeled to determine criterion for pitch stability.

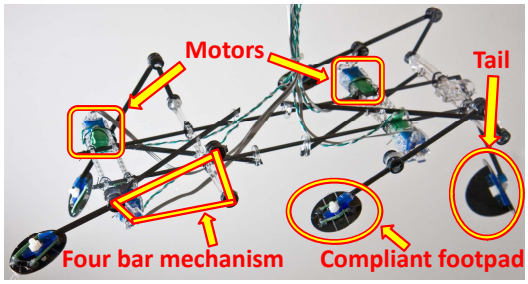

Fig. 1. Photograph of the four-legged robot inspired by basilisk lizards.

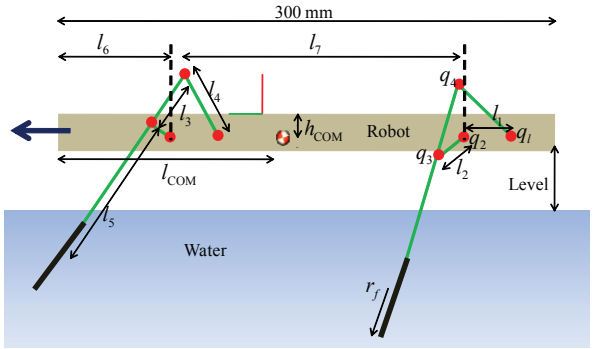

Fig. 2. Geometry and dimensions of the robot: Lengths of the four bar linkage is presented in TABLE I.

Robot Specification		Link Length	
Robot Length (m)	0.3	l_1 (m)	0.0615
Robot Width (m)	0.125	l_2 (m)	0.0218
Robot Mass (kg)	0.085	l_3 (m)	0.0748
Moment of Inertia		l_4 (m)	0.0468
Roll (kg m^2)	2.05×10^{-4}	l_5 (m)	0.0624
Pitch (kg m^2)	1.08×10^{-3}	l_6 (m)	0.01
Yaw (kg m^2)	1.24×10^{-3}	l_7 (m)	0.17325
Center of Mass (COM) and Footpad		l (m)	0.1894
l_{COM} (m)	0.127	l_t (m)	0.1
h_{COM} (m)	0.002		
r_f (m)	0.02		

TABLE I

ROBOT SPECIFICATIONS AND DIMENSIONS.

II. ROBOT MODEL DESCRIPTION

The water running robot has a mass of about 100 g, contains four miniature DC motors, and has four legs as shown in Fig. 1. It is 300 mm long, 125 mm wide, with much of the mass concentrated in the motors, located far from the center of the robot, as shown in Fig. 2. Each leg is driven by one motor, and employs four-bar mechanisms so that the foot trajectory of the robot mimics that of basilisk lizards. Each foot is a circle, 40 mm in diameter, with directional compliance which allows it to hit the water while flat, and fold during pullout, reducing undesired drag effects [13].

Four velocity controllers are employed in the simulation model, one for each motor, which apply an input torque. These controllers compute the errors of acceleration, velocity, and position, and apply the critical gain necessary to make the error in velocity converge to zero as quickly as possible. Furthermore, to have more precise control, a dynamic control input computed by inverse dynamics is applied to the model so the robot is able to achieve a better velocity profile.

III. KINEMATICS AND DYNAMICS

The robot kinematics and dynamics are formulated using recursive body kinematics and accumulated multibody system method, respectively [14]–[16]. Each joint's angle, velocity, and acceleration are derived using forward kinematics, and Jacobian matrices relate kinematic properties. Dynamics of the robot are derived from the principle of dynamic balance, which utilizes the Newton-Euler equation for single body motion and yields an equation of motion for the composite system by using D'Alembertian wrench [16].

Water interaction forces can be modeled as a combination of hydrostatic and hydrodynamic forces by applying an air cavity assumption [17]–[20]. By dividing the footpad's area into infinitesimal areas, the force and moment at a point can be derived numerically by multiplying hydrostatic and hydrodynamic pressure with the area. Integrating the force and the moment over the submerged area, the total water interaction force can be obtained [14].

A. Pitch Dynamics

As shown in Fig. 3, f_{x1}, f_{y1}, and f_{x2} generate pitch moments in a clockwise direction while only f_{y2} generates a counter-clockwise pitch moment. Most legged robots use redundant joints to place the center of mass (COM) or the zero moment point (ZMP) at desired positions which can achieve balance [21], [22]. However, the water runner cannot have several redundant actuators and links due to critical limitations on its weight. All four legs are needed for generating lift and propulsion forces, so pitch is not controllable with a simple quadrupedal robot body design, and a tail is suggested for stability.

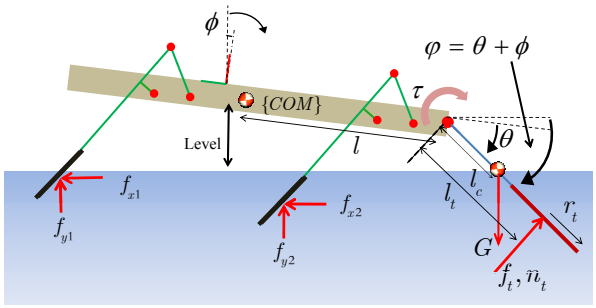

Fig. 3. A tail is proposed to control the pitch moment using hydrodynamic drag forces. Specified dimensions are in TABLE I.

B. Tail Dynamics

For the purposes of simulation, the tail is assumed to be made of light material and does not shift the location of the combined COM. Unlike the footpad, the motion of the tail is assumed to be sufficiently slow that no air cavity is created, and hydrostatic drag forces are not a concern. The hydrodynamic pressure exerted on the tailpad is derived from the viscous drag equation:

$$F_D(x,y) = \frac{1}{2} C_D \rho v_n^2 dxdy \tag{1}$$

where $F_D(x,y)$ is the drag force exerted at some point (x,y), $C_D \approx 1.1$ is a drag coefficient for a flat circle in submerged flow [23], ρ is the density of water, v_n is the velocity of the fluid in the direction normal to the tailpad, and $dxdy$ is an infinitesimally small area. The area of the tailpad is divided into infinitesimal area segments and each segment contains a reference frame so that one can find its normal velocity and position, and the force is integrated using the circular geometry to simplify:

$$\begin{aligned} f_t &= C_D\rho \int_0^a \sqrt{r_t^2 - (s-r_t)^2}\, v_n(s)|v_n(s)|\mathrm{d}s \\ &= C_D\rho \sum_{k=0}^{k\Delta<a} \Delta\sqrt{r_t^2 - (k\Delta - r_t)^2}\, v_{n,k}|v_{n,k}| \end{aligned} \tag{2}$$

$$\begin{aligned} n_t &= C_D\rho \int_0^a (s-r_t)\sqrt{r_t^2 - (s-r_t)^2}\, v_n(s)|v_n(s)|\mathrm{d}s \\ &= C_D\rho \sum_{k=0}^{k\Delta<a} \Delta(k\Delta - r_t)\sqrt{r_t^2 - (k\Delta - r_t)^2}\, v_{n,k}|v_{n,k}| \end{aligned} \tag{3}$$

where

$$v_n(s) = v\sin\varphi + (l_t + r_t - s)\dot{\varphi}$$
$$v_{n,k} = v\sin\varphi + (l_t + r_t - k\Delta)\dot{\varphi}$$
$$\varphi = \theta + \phi$$

where f_t and n_t are the force and the moment, respectively, generated by the tail and taken at the center of the tailpad, r_t is the radius of the tailpad shown in Fig. 3, Δ is a discretized length which determines the precision of integration, l_t is the length from the tail's attachment point to the body to the center of the tailpad, θ is the tail's angle relative to the robot body, ϕ is the pitch angle of the robot body, and v is horizontal robot body velocity as shown in Fig. 3. The interval of integration can be determined by the following:

$$a = \begin{cases} h & \text{if } |h| < 2r_t \\ 2r_t & \text{if } |h| \geq 2r_t \end{cases}$$

where h is the distance from the lowest point of the tail to the surface of the water within the tail's reference frame, and r_t is the radius of the tailpad. The dynamics of the tail angle and the pitch angle can be described:

$$\ddot{\theta} = \frac{1}{\mathcal{I}}(\tau - l_t f_t(\varphi, \dot{\varphi}) - l_c G\sin\varphi) \quad (4)$$
$$\ddot{\phi} = \frac{1}{\mathcal{I}_p}(n_{COM} - n_{tail}) \quad (5)$$
$$n_{tail} = n_t + p_{tail} \times f_t \quad (6)$$

where $f_t(\varphi, \dot{\varphi})$ and G are forces acting on tailpad from (2) and gravity, respectively. $\mathcal{I}$ is the moment of inertia of the tail and l_c is the length from the tail from the attachment point to the body to the tail's center of mass (Fig. 3). n_{tail} is the moment generated by the tail measured at the COM, p_{tail} is translation vector from the COM to the tailpad, n_{COM} is the moment around the center of mass caused by water interactions with the feet, and $\mathcal{I}_p$ is the pitch moment of inertia of the robot.

IV. Tail Modeling

The simulated pitch moment, n_{tail}, generated by the tail and measured at the COM with respect to the angle between tail and water surface, φ, can be approximated as

$$n_{tail} \approx \begin{cases} 0 & \text{if } \varphi \leq \varphi_{min} \\ n_{gt} & \text{if } \varphi > \varphi_{min} \end{cases} \quad (7)$$

where

$$n_{gt} = \frac{1}{2}C_D\rho\pi r_t^2(l\cos\theta + l_t)(v\sin\varphi)^2 A$$
$$A = \begin{cases} \frac{r_t + l_t - y/\sin\varphi}{2r_t} & \text{if } (r_t + l_t - y/\sin\varphi) < 2r_t \\ 1 & \text{if } (r_t + l_t - y/\sin\varphi) \geq 2r_t \end{cases}$$
$$\varphi_{min} = \sin^{-1}\left(\frac{y}{l_t + r_t}\right)$$
$$y = Level - l\sin\phi$$

A is the ratio of the submerged area and φ_{min} is the minimum tail angle required to generate a water interaction based on robot geometry and position relative to the water.

In simulation, the robot is free to rotate about the pitch axis at the COM but is constrained in all other directions such as roll and yaw. Horizontal velocity of the robot is assumed to be 1 m/s, which has been achieved in experimental trials.

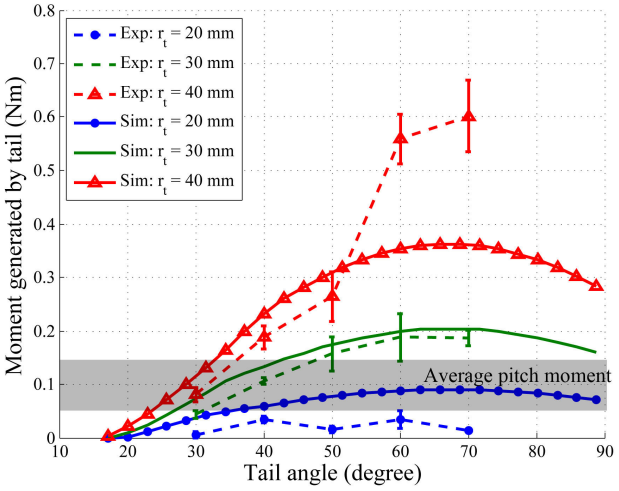

Fig. 4. Experiment and simulation results of pitch moment generation, n_{tail}, at a running frequency of 7 Hz. The moment generated by the tail can be approximated by (7) as a function of r_t, v and φ. The minimum tail radius which can generate enough pitch moment is slightly less than 30 mm.

A. Passive Tail

The objective of the tail is to generate enough counter-clock wise pitch moment (Fig. 3) to negate the clockwise pitch moment generated by the four feet. Also, it should be able to make the average pitch angle of the robot zero. For simplicity, we first propose a passive, circular tail which is attached at the end of the robot body at an angle. Figure 4 shows the pitch moment generated by a tail with varying tail angles, radii, and running speeds for a horizontal robot body.

If the horizontal force generated by the tail, f_{t_x}, is greater than average propulsion force generated by legs, $\overline{f_p} = 0.68\ N$, it will decelerate the robot. In order for $f_{t_x} < \overline{f_p}$, the tail angle, φ, should be limited. f_{t_x} can be approximated by:

$$f_{t_x} \approx \frac{1}{2}C_D\rho\pi r_t^2 v^2(\sin\varphi)^3 A \quad (8)$$

Since the average pitch moment generated by the water interaction is known to be 0.08 Nm ~ 0.14 Nm, the minimum radius of a tail which can produce this pitch moment is about 20 mm. To choose the appropriate tail angle, Fig. 6 was used. It shows the average of the offset pitch angle when a certain tail angle is applied. $30° - 33°$ of a 30 mm radius of tail maintains the robot posture near a zero pitch angle. Figure 7 shows the result of the pitch motion with the passive tail.

B. Active Tail

The passive tail can generate the required average pitch moment to stabilize the pitch motion of the robot in steady state. However, if there is a disturbance, i.e. varying horizontal velocity and/or changing the average pitch moment

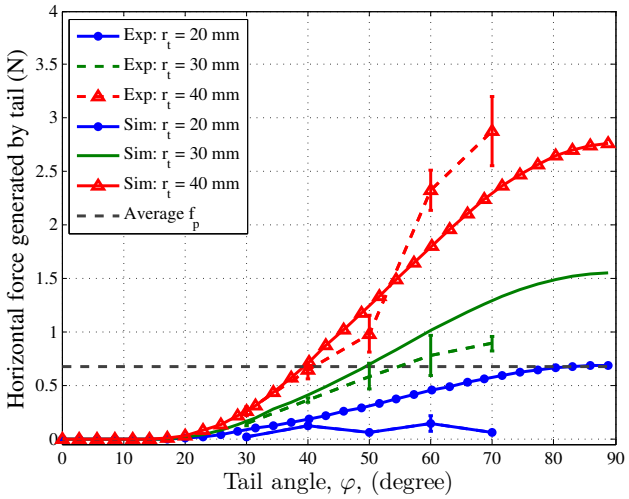

Fig. 5. To satisfy $f_{t_x} < \overline{f_p}$ criterion, the tail angle should be limited.

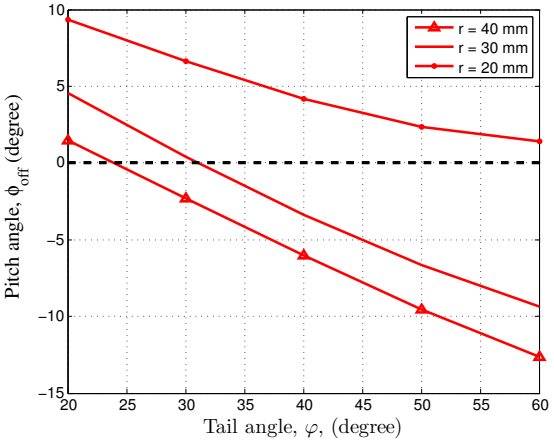

Fig. 6. The average body pitch angle offset, ϕ_{off}, can be a criterion for choosing the tail angle, θ. When $\phi_{off} = 0$, the tail angle necessary to cancel the net pitch moment around the center of mass can simultaneously make the robot body horizontal.

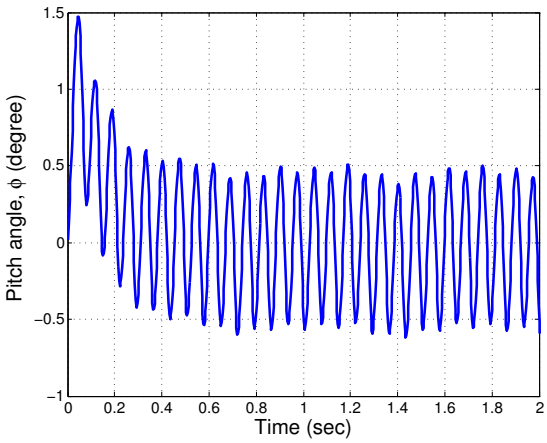

Fig. 7. When $r_t = 30\ mm$ and $\theta = 31°$, the average pitch angle offset, ϕ_{off}, becomes almost zero and the pitch motion with a passive tail is stable.

by adjusting the gait of the robot, there is no way to control the robot pitch or recover its initial body orientation. In order to cope with this, an active tail to control pitch motion using sensory feedback is proposed. This tail should cancel the net pitch moment around the COM and also correct the robot's posture. By measuring the angular acceleration around the center of mass, and knowing the inertia matrices, the pitch moment around the COM can be deduced, and the desired pitch moment the tail should generate to balance the robot's posture can be computed. Then, the desired tail angle can be determined by solving the nonlinear equation (7) using a Newton-Raphson nonlinear equation solver. We propose a moment average tracking PD controller by applying torque at the tail joint:

$$\tau = -k_p(\varphi_d - \theta) - k_d(-\dot{\theta}) - l_c G \sin\varphi \qquad (9)$$

where

$$\varphi_d = \texttt{NRsolve}(n_d)$$
$$n_d = n_{tail} + \frac{1}{T}\int_{t-T}^{t} n_{tail} - n_{COM}\mathrm{d}t$$

$\texttt{NRsolve}(n_d)$ is Newton-Raphson nonlinear equation solver which returns a solution corresponding to the equation n_d, the desired moment from the tail. The reason why θ appears instead of φ in (9) is that this can rectify its posture, *i.e.* $\varphi_d = \theta_d$, if $\phi \to 0$ as $t \to \infty$. T is the period of time to take an average.

The desired moment is the sum of the estimated moment generated by the current tail angle and the average pitch moment at the COM. The average moment at the COM represents the overall net pitch moment which makes the robot gradually tilt backwards. Integrating the moment measured at the COM, the pitch motion of the robot becomes more stable and robust since it does not have to track noise and high frequency vibrations due to the motion of the legs. Little or no motion of the tail angle (Fig. 8), θ, can control the robot pitch moment. (After all, the controller becomes similar to a passive tail if $T \to \infty$.) Since the variations of θ are small, the base body pitch angle also becomes more stable, as shown in Fig. 9. However, simply increasing T causes slow responses to disturbances. Therefore, one should carefully select a value of T that is appropriate for the system.

By taking an appropriate PD gain, $k_p = 1$ and $k_d = 0.007$, the tail angle, θ, can be controlled to track a desired angle, φ_d so as to negate the instantaneous pitch moment at the COM. This controller results in stable pitch motion with a maximum pitch angle variation $\pm 1°$ at steady state.

C. Velocity Estimator

Since the pitch moment equilibrium point can be different from the point where the pitch angle, ϕ, becomes zero, shown in Fig. 9, an additional controller that negates any offset in ϕ is necessary. Also, if the robot's horizontal velocity is not constant, the solution of the nonlinear equation (7) can be inaccurate. To account for these, a velocity estimator which updates the current horizontal velocity by measuring ϕ is

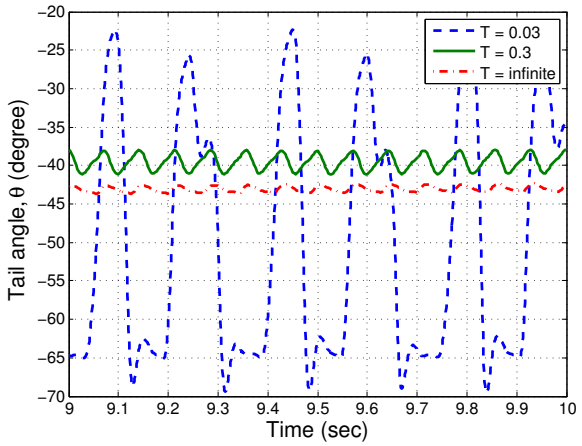

Fig. 8. Increasing T reduces variation of tail angle, θ, so that pitch motion can be controlled without high vibration of tail. When T is 0.3 sec, variation is about 5° and the controller becomes more realizable.

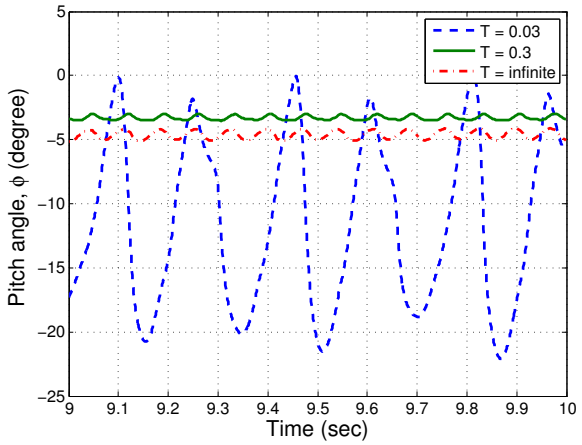

Fig. 9. As increasing T, variation of base body pitch angle, ϕ, is reduced. When T is 0.3 sec, it becomes less than 3°. Note that there is ϕ offset. In order to get rid of it, the velocity estimator is introduced.

proposed. If the actual velocity v is reduced, the average ϕ becomes greater due to the fact that the current tail angle, θ, is insufficient to generate the necessary stabilizing pitch moment. This tends to make the robot become inclined with an offset of ϕ. In order to correct its posture, the robot needs to estimate how much v is reduced and apply more torque to the tail so as to maintain a steeper θ, and vice versa for increased v. The velocity estimator is updated as follows:

$$v = v + k_{v_p}\phi + k_{v_d}\dot{\phi} \tag{10}$$

where k_{v_p} and k_{v_d} are PD gains. This estimator can cope with varying v and also removing the ϕ offset. Fig. 10 shows the velocity estimator tracking the actual v. There is an offset in the estimated velocity, $v_{off} \sim 0.2$ m/s, but still corrects the offset in body orientation, ϕ.

Figure 11 shows comparison between the active tail and passive tail. At the beginning of simulation, huge pitch angle displacement ($\sim 18°$) is occured to compensate sudden step response of pitch moment generated by feet. Also at this

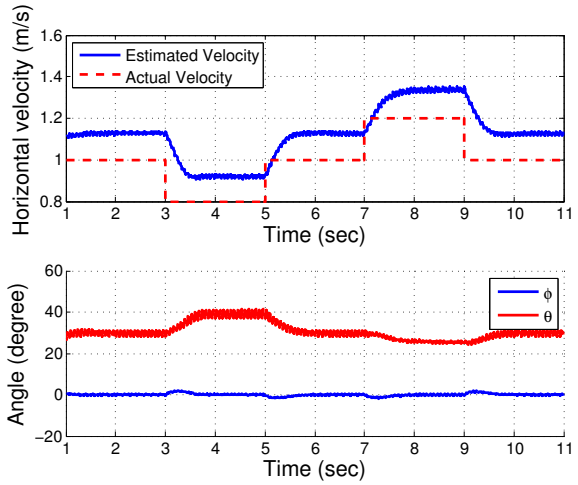

Fig. 10. When the actual base body velocity, v, is varying, the solution from the nonlinear equation is inaccurate, because it assumes $v = 1.0$ m/s. By estimating v using (10), which penalizes any ϕ offset, the robot can cope with disturbances. The actual velocity v is changed every 2 seconds. Note the pitch angle, ϕ, always becomes zero by controlling the tail angle, θ.

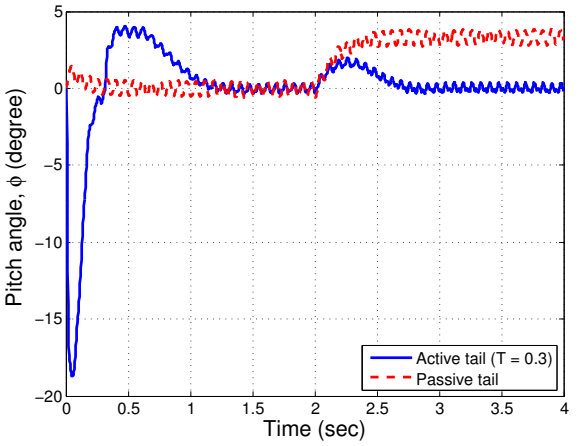

Fig. 11. Unlike the passive tail, the active tail can deal with disturbances using information of the net pitch moment at the COM and the pitch angle. The velocity is decreased at time $t = 2.0$ s from 1.0 m/s to 0.8 m/s.

moment, since duration of integration is too short, φ_d is changed highly so it results in high pitch angle displacement. However, it converges to steady state value after 1 second. At $t = 2.0$ sec, the disturbance which is the horizontal velocity variation is applied but the controller negates ϕ. Whereas, passive tail cannot deal with such a disturbance so the steady state value is not $\phi = 0$.

V. Discussion and Future Work

Depending on the gait of the robot, the magnitude of pitch moment can be varied. In this paper, we simulated with the worst case gait scenario, a trot gait, in which diagonal feet are synchronized and touch the water simultaneously. In reality, a different gait could be utilized, such as a hopping (all four feet synchronized) or pace (two lateral feet in phase) gait. Since the controller is designed to manage the worst gait

case, the variation of the tail angle and the pitch angle will likely be reduced for other gaits.

Since moment/tail angle relation at the vicinity of the operating point (average pitch moment in Fig. 4) is somewhat linear, one may claim that a standard linear controller described in terms of the pitch angle, ϕ, can replace the Newton-Rapson nonlinear equation solver applied in (9) without a velocity estimator. However, as shown in (7), the pitch moment is function of a not only ϕ but also θ which is not taken into account in a linear controller. Thus, the applied torque at the tail cannot be related to the tail angle, which might move the operating point to a point where it ceases to be linear. Also, disturbances can change the pitch moment generation for a given tail angle. To resolve these problems, an adaptive controller that updates gains depending on ϕ, θ, and v is inevitable. We integrate all functions into the Newton-Rapson nonlinear equation solver with a velocity estimator by choosing the gains carefully.

In order to realize the moment average controller, we are planning to implement an accelerometer and a gyroscope sensor at the COM of the robot to measure the pitch axis angular acceleration and the pitch angle. Micro DC motors will be used to actuate the tail joint. The reason we use a circular tailpad is its drag coefficient is relatively high compared to other geometries such as rectangular or elliptical. However, there are several different geometries which have even higher drag coefficients, such as a hollow hemisphere. Thus, if we can use one of these geometries for a tailpad, it may be possible to reduce the size. Furthermore, designs such as hydrofoils that rely on speed induced pressure differences are unlikely to work due to the low running velocities. In addition, for yaw motion and increased stability in the roll direction, a tail with a rudder can be introduced for the next generation of tail.

Also, it was initially assumed that the tail would move slowly enough through the water that no air cavity would form behind it. If this assumption proves to be untrue, the tail would provide more restorative force than predicted, and either a more shallow angle or a smaller diameter tail could be used to achieve stability in the pitch direction. For small changes in angle, such an effect can be taken into account by increasing the effective drag coefficient or modifying the tail moment equation (7) with a correction factor.

VI. Conclusion

The pitch motion of bio-inspired water running robot was unstable due to unbalanced moment at the COM. In order to stabilize, a tail which enable to compensate moment at the COM is introduced. We propose two types of the tails, passive and active tails. The passive tail is fixed at the end of the robot body with a certain tail angle and radius. Average pitch moment provides clue to choose the radius of the tail and average pitch offset angle shows which tail angle is appropriate. Nevertheless, since the passive tail cannot take into account for disturbance, the active tail angle which can generate enough pitch moment to cancel net pitch moment at the COM. In order to find the desired tail angle, average pitch moment as varying, T, is studied for feasibility and response of the robot. Additionally, velocity estimator calibrates pitch angle, ϕ, offset and tracks actual velocity so that it enables to cope with horizontal base body velocity changes.

References

[1] R. Suter *et al.*, "Locomotion on the water surface: Propulsive mechanisms of the fisher spider *Dolomedes Triton*," *J. of Exp. Biology*, vol. 200, pp. 2523–2538, October 1994.

[2] Y. S. Song and M. Sitti, "Surface tension driven biologically inspired water strider robots: Theory and experiments," *IEEE Trans. on Robotics and Automation*, vol. 23, pp. 578–589, June 2007.

[3] J. Bush and D. Hu, "Walking on water: Biolocomotion at the interface," *Annual Rev. of Fluid Mech.*, vol. 38, pp. 339–369, January 2006.

[4] S. Floyd, T. Keegan, and M. Sitti, "A novel water running robot inspired by basilisk lizards," in *Proc. of the 2006 IEEE/RSJ Int. Conference on Intelligent Robots and Systems*, Beijing, China, November 2006, pp. 5430–5436.

[5] A. Boxerbaum, P. Werk, D. Quinn, and R. Vaidyanathan, "Design of an autonomous amphibious robot for surf zone operation," in *Proc. of the IEEE/ASME International Conference on Advanced Intelligent Mechatronics*, July 2005, pp. 1459–1464.

[6] A. Crespi, A. Badertscher, A. Guignard, and A. Ijspeert, "Amphibot 1: an amphibious snake-like robot," *Robotics and Autonomous Systems*, vol. 50, pp. 163–175, March 2005.

[7] S. Guo, T. Fukuda, and K. Asaka, "A new type of fish-like underwater microrobot," *IEEE/ASME Trans. on Mechatronics*, vol. 8, pp. 136–141, March 2003.

[8] C. Georgiadis, "Aqua: An aquatic walking robot," in *Proc. of the IEEE/RSJ International Conference on Intelligent Robots and Systems*, September 2004, pp. 3525–3531.

[9] Y. Song, S. Suhr, and M. Sitti, "Modeling of the supporting legs for designing biomimetic water strider robots," in *Proc. of International Conference on Robotics and Automation*, May 2006, pp. 2303–2310.

[10] D. Hu, B. Chan, and J. Bush, "The hydrodynamics of water strider locomotion," *Nature*, vol. 424, pp. 663–666, August 2003.

[11] H. Takonobu, K. Kodaira, and H. Takeda, "Water striders muscle arrangement-based robot," in *IEEE/RSJ International Conference on Intelligent Robots and Systems*, August 2005, pp. 1754–1759.

[12] S. Floyd and M. Sitti, "Design and development of the lifting and propulsion mechanism for a biologically inspired water runner robot," *IEEE Transactions on Robotics*, vol. 24, no. 3, pp. 698–709, June 2008.

[13] S. Floyd, S. Adilak, R. Rogman, and M. Sitti, "Performance of different foot designs for a water running robot," in *Proc. of International Conference on Robotics and Automation*, 2008, pp. 244–250.

[14] H. S. Park, S. Floyd, and M. Sitti, "Dynamic modeling of a basilisk lizard inspired quadruped robot running on water," in *Proc. of the IEEE/RSJ Int. Conference on Intelligent Robots and Systems*, 2008, pp. 3101–3107.

[15] R. M. Murray, Z. Li, and S. S. Sastry, *A Mathematical Introduction to Robotic Manipulation*. CRC Press, Inc., 1994.

[16] J. Park, "Principle of dynamical balance for multibody systems," *Multibody System Dynamics*, vol. 14, pp. 269–299(31), November 2005.

[17] J. Glasheen and T. McMahon, "Vertical water entry of disks at low froude number," *Phys. of Fluids*, vol. 8, pp. 2078–2083, August 1996.

[18] J. W. Glasheen and T. A. McMahon, "A hydrodynamic model of locomotion in the basilisk lizard," *Nature*, vol. 380, pp. 340–342, 1996.

[19] S. T. Hsieh and G. V. Lauder, "Running on water: Three-dimensional force generation by basilisk lizards," *PNAS USA*, vol. 101, pp. 16 784–16 788, November 2004.

[20] S. T. Hsieh, "Three-dimensional hindlimb kinematics of water running in the plumed basilisk lizard (*Basiliscus plumifrons*)," *J. of Experimental Biology*, vol. 206, pp. 4363–4377, August 2003.

[21] S. Kajita *et al.*, "Biped walking pattern generation by using preview control of zero-moment point," in *Proc. of the IEEE Int. Conference on Robotics and Automation*, September 2003, pp. 1620–1626.

[22] J. Park and Y. Youm, "General zmp preview control for biped walking," in *Proc. of the IEEE Int. Conference on Robotics and Automation*, April 2007, pp. 2682–2687.

[23] B. R. Munson, D. F. Young, and T. H. Okiishi, *Fundamentals of fluid mechanics*. John Wiley and Sons, Inc., 2002.